Acta Oceanol. Sin., 2019, Vol. 38, No. 11, P. 158–161
https://doi.org/10.1007/s13131-019-1506-3
http://www.hyxb.org.cn
E-mail: hyxbe@263.net

News and Views

China-France Oceanography Satellite (CFOSAT) simultaneously observes the typhoon-induced wind and wave fields

Ying Xu[1, 3], Jianqiang Liu[1, 3], Lingling Xie[2]*, Congrong Sun[1, 3], Jinpu Liu[1, 3], Junyi Li[2], Di Xian[4]

[1] National Satellite Ocean Application Service, Ministry of Natural Resources, Beijing 100081, China

[2] Guangdong Key Laboratory of Coastal Ocean Variability and Disaster Prediction, Guangdong Ocean University, Zhanjiang 524088, China

[3] Key Laboratory of Space Ocean Remote Sensing and Application, Ministry of Natural Resources, Beijing 100081, China

[4] National Satellite Meteorological Center, China Meteorological Administration, Beijing 100081, China

Received 18 October 2019; accepted 21 October 2019

© Chinese Society for Oceanography and Springer-Verlag GmbH Germany, part of Springer Nature 2019

The China-France oceanography satellite (CFOSAT) developed by the China National Space Administration (CNSA) and Centre National D'Etudes Spatiales (CNES) was successfully launched into its orbit on October 29, 2018. The Chinese wind scatterometer (SCAT) with swath width of about 1 000 km and French wave spectrometer (Surface Wave Investigation and Monitoring, SWIM) with swath width of about 180 km onboard the CFOSAT are in line with all requirements and performing operationally. Thus, it is the first time that CFOSAT provides simultaneous and co-located observations of wind and wave fields with high spatial resolutions of 12.5 km×12.5 km for the winds and 70 km×90 km for the wave directional spectrum. The real-time and large-scale monitoring of wind and wave fields are of great significance for navigation and human activities on the sea (Xu et al., 2010; Tan et al., 2018; Sun et al., 2019), especially during severe typhoon processes when violent winds and hazardous waves occur (Walsh et al., 2002; Zhou et al., 2008).

Super typhoon Lingling (2019) is a strong typhoon passing over the China offshore waters in 2019. It was born as a tropic storm in the Northwest Pacific east of Luzon Island on September 2, 2019, and enhanced to be a super typhoon in east of Taiwan Island as passing over the warm Kuroshio water on September 5 (Fig. 1). It moved northward along 125°E, crossed the East China Sea and landed on the western coast of Korea Peninsula on September 7.

The CFOSAT met typhoon Lingling (2019) and measured wind and wave fields at about 10:22 UTC on September 4. Figure 1a shows the distribution of the CFOSAT observed wind vectors along track 4701 from the equatorial West Pacific to the Bohai Sea and the Japanese Sea. One can see cyclonically rotating wind vectors with wind speeds higher than 20 m/s on the open ocean southeast of Taiwan Island. The typhoon center was detected at 22°41′41″N, 125°19′19″E, and the radius of wind moderate gale was about 270 km. The maximum wind speed reached above 24 m/s, and the radius of the maximum wind (RMW) was about 50 km. Outside the wind gale range, the wind speeds decreased to about 10 m/s at a distance of 500 km, i.e., ten times of the RMW from the typhoon center. The wind directions were mostly northwestward on the right side of the typhoon track in the open ocean of the Northwest Pacific and the East China Sea between 18° and 30°N. Beyond the range, the wind speeds gradually decreased. In the southeast, another tropic low pressure 92W with wind speed of about 15 m/s was visible in east of Mindanao Island, Philippines.

Figure 1b shows the simultaneous CFOSAT observation of wind fields, nadir significant wave heights (SWHs) and wave spectrum parameters during typhoon Lingling. The background is a Chinese Fengyun-4A (FY-4A) AGRI (Advanced Geostationary Radiation Imager) image acquired at 9:00 UTC on the same day. One can see that the spiral cloud system from visible image is consistent with the cyclonic wind field from CFOSAT scatterometer, as well as the detected typhoon center. We further compare the CFOSAT wind vectors to the remote sensed surface winds from CMEMs two hours later at 12:00 UTC on September 4, 2019 (http://marine.copernicus.eu). As shown in Fig. 1c, the two wind fields are similar, and the mean difference of wind speeds is 1.1 m/s.

Figure 2 shows the observations of SWHs, dominant wave directions and dominant wave length along two sub-tracks on the right side of the typhoon track from the Philippine Islands to the southern part of Korea Pennisula. From Fig. 2a, we can see that the waves are generally higher than 4 m inside the ten-RMW circle at latitudes between 20°N and 25°N. The maximum spectrum SWH reaches 5.2 m at grids nearest the typhoon, and decreases with the distance from the typhoon center. In north of 28°N and south of 16°N, the SWHs decrease to about 1.5–2.5 m, still 2–6 times larger than the climatologic values of 0.4–1 m in the Northwest Pacific in autumn (Li et al., 2012). Comparing to the spectrum SWHs, the CFOSAT nadir SWHs (dots with black) have similar spatial variation with larger values inside the ten-RMW circle of the typhoon, while the nadir SWHs are generally 1 m lower than the spectrum measurements. The Chinese Haiyang-2B (HY-2B) nadir SWHs are also overlaid for comparison. The two values of nadir observations are similar to each other with mean difference of 0.3 m.

The wavelengths of the dominant waves are derived from the SWIM observations. As shown in Fig. 2b, the wavelengths are

Foundation item: The National Natural Science Foundation of China under contract Nos 41506207, 41776034 and 41706025; the GASI Project under contract No. GASI-02-SCS-YGST2-02; the Guangdong Province High Education Improving Plan under contract No. CYL231419012.

*Corresponding author, E-mail: llingxie@163.com

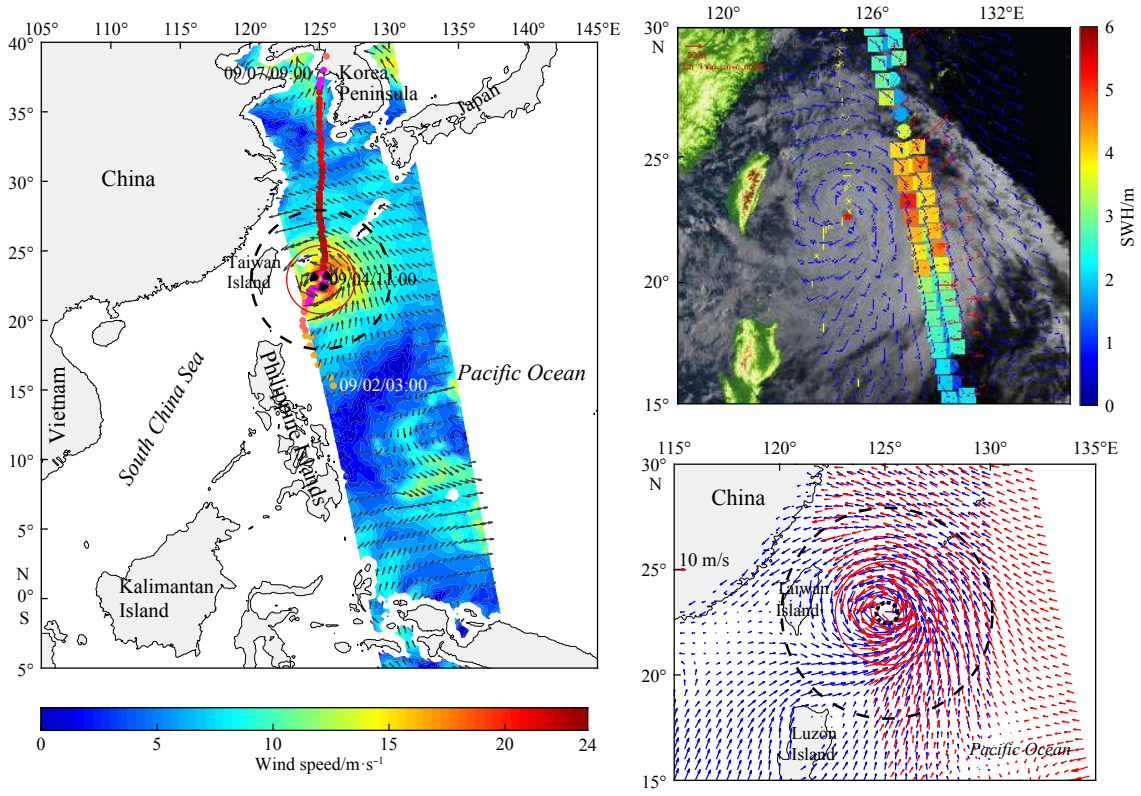

Fig. 1. Simultaneous observation of wind and wave fields by the CFOSAT. a. Wind speeds (color shading) and vectors (grey arrows) observed by the CFOSAT along track 4701. Red circle represents the typhoon radius of 270 km with moderate gale. Dotted black circle represents the radius with maximum wind (RMW) of 50 km. Dashed black circle represents the ten-RMW circle. Numbers on the typhoon track (color dots) are dates (mm/dd/hh). b. Simultaneous CFOSAT observations of wind fields (blue wind barbs), dominant wave directions with wavelength (red arrows) and significant wave heights (SWHs) (color squares as spectrum measurements and color dots as nadir measurements) observed by the CFOSAT (typhoon center on 10:22:17 UTC on September 4, 2019). Red pentagram indicates the typhoon center and yellow stars represent the typhoon track. The background cloud image is a Chinese FY-4A AGRI image acquired at 9:00 UTC on September 4, 2019. c. Comparison of CFOSAT wind vectors (red arrows) to CMEMs wind vectors (blue arrows).

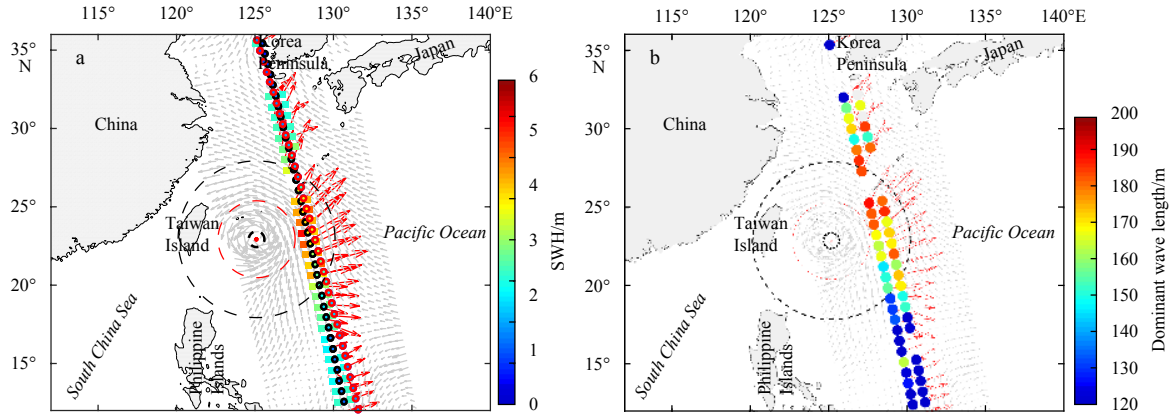

Fig. 2. Distribution of wave parameters along CFOSAT track. a. Distribution of CFOSAT spectrum SWHs (color squares) and nadir SWHs (dots with black circle, left) with wave propagation direction (red arrow). HY-2B nadir SWHs are overlaid (dots with magenta circle, right) for comparison; b. distribution of CFOSAT spectrum wave lengths (color dots) with wave propagation direction (red arrow). Grey arrows represent the simultaneous wind vectors.

in a range of 120–200 m, and have an increase trend from 15°N to 28°N. There are larger values of 150–180 m inside the ten-RMW circle between 20°N and 25°N, and smaller values of 120–130 m in the north of 30°N and south of 15°N. According to the deep-water wave theory, the group velocities of the observed waves are in range of 6.8–8.8 m/s. The mean value is 8.1 m/s for a mean wave length of 170 m.

For the wave direction, one can see that the waves mostly propagate eastward on the right side of the typhoon track, while the wind directions are mostly northwestward. The wave directions turn to more northeastward in the north and a little southeastward in the south, but still misalign the wind vectors. Previous investigators have addressed that misalignment of local winds and propagating waves occurs commonly due to the curvature in the typhoon wind fields (Xu et al., 2017). Moon et al. (2003) pointed out that the deviation between the wind direction and the wave direction increases with the distance from the RMW. They derived the angle θ between the wave direction and the wind direction as $\theta=\cos^{-1}(a/x)$ $(x\geqslant a)$, where a is the RMW, and x is the distance from the typhoon center. Taking a=50 km, the theoretical deviations are calculated for distance x from 50 to 500 km.

Figure 3a shows comparison of the observed wave heights with the latitudes along the sub-track (dots) with the estimated values $h_{\mathrm{PM}} \approx 0.22\frac{(U_{10})^2}{g}$ based on the Pierson-Moskowitz spectrum, where U_{10} is the wind speed at 10 m, and g is the gravity acceleration (curves) (Stewart, 2008). The estimates are close to the spectrum observations at a high state with wind speeds larger than 14 m/s near the typhoon center at 20°–25°N (blue curve). Beyond this range, there is a bias of 1–2 m in lower sea state with winds lower than 10 m/s for the spectrum SWHs. For the nadir SWHs, they are closer to the theory estimation in lower sea state, but missed the highest value in high state.

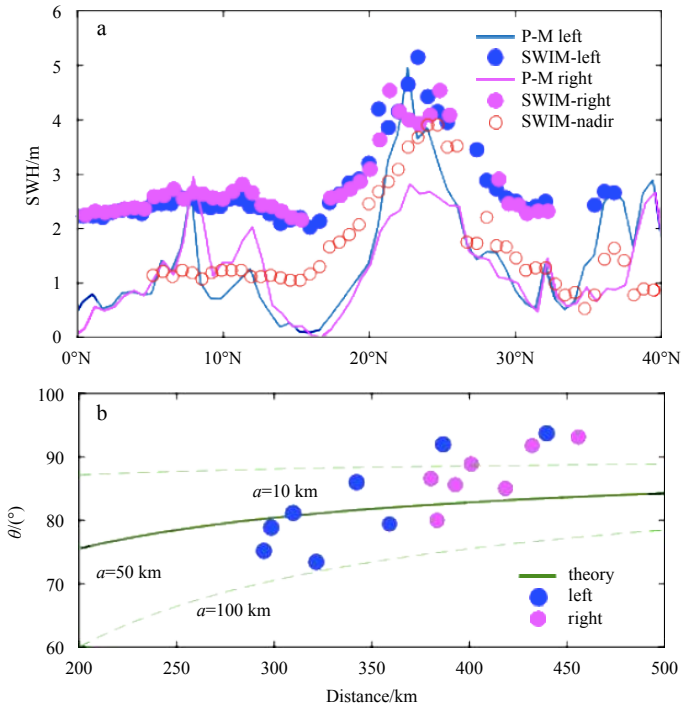

Fig. 3. Comparison of theoretical estimates and the CFOSAT observations. a. Comparison of CFOSAT observed SWHs (solid dots for spectrum measurements, circles for nadir measurements) and estimated SWHs (curves) along the left (blue) and right (magenta) SWIM sub-tracks. The estimations are based on the Pierson-Moskowitz spectrum. b. Comparison of theoretical (curves) and observed (dots) deviation angles between the wind directions and wave directions with the distance from the typhoon center. Blue and magenta dots and curves represent that from the left and right SWIM sub-tracks, respectively.

Figure 3b shows the comparison of theoretical deviation angles (solid green curve) with the observed deviation angles (dots) in the typhoon affected area from 20° to 28°N. Theoretical results with a=10 and 100 km are also presented (dashed green curves). One can see that the CFOSAT observed data points are mostly located between the theoretical curves. The correlation coefficient between the theoretical results with a=50 km and the observations reaches 0.95 and 0.80, respectively.

This study is a preliminary test, which aims to extract the wind and wave characteristics during passage of super typhoon Lingling (2019) over the Northwest Pacific and China offshore waters from the high-spatial-resolution, simultaneous observations of winds and waves by the CFOSAT. The results show that the observed SWHs generally agree with the theoretical estimates in high sea state. The misalignment of the wind and wave directions during typhoon was observed, and the deviation angle increases with the distance from the typhoon center as theoretically predicted. These results provide good examples for applications of the CFOSAT measurement data.

Acknowledgements

All CFOSAT data are provided by courtesy of CNSA and CNES. The CFOSAT and HY-2B data is downloaded from https://osdds.nsoas.org.cn. The typhoon track data are downloaded from http://typhoon.weather.com.cn/index.shtml. The topography data are download from https://www.ngdc.noaa.gov/mgg/global/etopo2.HTML. FY-4A AGRI data is downloaded from http://data.

nsmc.org.cn. We thank Dongliang Shen, Peng Bai, Mingming Li, Keyi Tan and Sijie Deng for discussion and help in data analysis.

References

Li Jing, Zhou Lin, Zheng Chongwei, et al. 2012. Spatial-temporal variation analysis of sea wave field in the Pacific Ocean. Marine Science, 36(6): 94–100

Moon I J, Ginis I, Hara T, et al. 2003. Numerical simulation of sea surface directional wave spectra under Hurricane wind forcing. Journal of Physical Oceanography, 33(8): 1680–1706, doi: 10.1175/2410.1

Stewart R H. 2008. Introduction to Physical Oceanography. Texas: Texas A & M University, 287

Sun Junchuan, Wei Zexun, Xu Tengfei, et al. 2019. Development of a fine-resolution atmosphere-wave-ocean coupled forecasting model for the South China Sea and its adjacent seas. Acta Oceanologica Sinica, 38(4): 154–166, doi: 10.1007/s13131-019-1419-1

Tan Keyi, Zhang Biao, Xie Lingling. 2018. Ocean wave parameter retrieval from satellite SAR with EMD method. Journal of Guangdong Ocean University, 38(4): 77–84

Walsh E J, Wright C W, Vandemark D, et al. 2002. Hurricane directional wave spectrum spatial variation at landfall. Journal of Physical Oceanography, 32(6): 1667–1684, doi: 10.1175/1520-0485(2002)032<1667:HDWSSV>2.0.CO;2

Xu Yao, He Hailun, Song Jinbao, et al. 2017. Observations and modeling of typhoon waves in the South China Sea. Journal of Physical Oceanography, 47(6): 1307–1324, doi: 10.1175/JPO-D-16-0174.1

Xu Qing, Lin Hui, Li Xiaofeng, et al. 2010. Assessment of an analytical model for sea surface wind speed retrieval from spaceborne SAR. International Journal of Remote Sensing, 31(4): 993–1008, doi: 10.1080/01431160902922870

Zhou Liangming, Wang Aifang, Guo Peifang. 2008. Numerical simulation of sea surface directional wave spectra under typhoon wind forcing. Journal of Hydrodynamics, 20(6): 776–783, doi: 10.1016/S1001-6058(09)60015-9